Fracture toughness and hydrogen embrittlement susceptibility on the interface of clad steel pipes with and without a Ni-interlayer

L. Jemblie[a,*], H. Bjaaland[a,1], B. Nyhus[b], V. Olden[b], O. M. Akselsen[a,b]

[a] *Department of Engineering Design and Materials, NTNU, 7456 Trondheim, Norway*
[b] *SINTEF Materials and Chemistry, 7456 Trondheim, Norway*

Abstract

The objective of the present work has been to study the fracture properties of the interface between clad and base material of two 316L austenitic stainless steel - X60/X65 carbon steel hot roll bonded clad pipes; with and without a Ni-interlayer. Fracture mechanical tests were performed in air and under in situ electrochemical hydrogen charging to establish crack growth resistance curves and fracture initiation toughness for both systems. The results revealed that an electroplated Ni-interlayer reduces the fracture initiation toughness for testing in air, while it raises the fracture initiation toughness for testing in hydrogen environment. The samples with a Ni-interlayer revealed little influence of hydrogen on the fracture resistance, with a reduction in the fracture initiation toughness of 20 %, attributed to crack propagation mainly occurring in the nickel layer. The samples without a Ni-interlayer revealed a strong influence of hydrogen on the fracture resistance, with a reduction in the fracture initiation toughness of 85 %. An alternating crack path was proven, shifting between the dissimilar interface and the base material adjacent to the interface.

Keywords: Clad pipe, Cladding, Hydrogen embrittlement, Fracture toughness, Electroplating, Interface

1. Introduction

Steel pipelines represents an important part of the subsea infrastructure for transport of unprocessed oil and gas. In areas facing high content of corrosion inducing products, there is a demand for pipes with a corrosion resistant interior, able to withstand environmental degradation and cracking during full service life. Composite pipes, where a corrosion resistant alloy (CRA) is internally bonded to a conventional carbon steel pipe, has become increasingly popular as an economical viable option for corrosion management, combining the mechanical properties of the structural steel with the corrosive properties of the CRA. This however offers new challenges with respect to integrity management and degradation assessment, due to an inhomogeneous material combination and a complex interface region.

Clad steel pipe refers to pipes where the bond between the base material (BM) and the CRA is metallurgical, as opposed to lined pipes, where the bond is mechanical. The principle manufacturing method combines hot rolling of clad plates to form the metallurgical bond, followed by bending into the shape of a pipe in a press bending process [1, 2]. During production, due to the wide difference in chemical composition between the base material and the clad layer, considerable transport of elements across the interface may occur. This is especially prominent for carbon, considering the element's high mobility. The resulting interface, while highly dependent on the production parameters, is microstructural complex with increased hardness and carbide precipitates on the clad side and carbon depletion followed by grain growth in the ferritic base metal [3, 4, 5, 6, 7, 8].

The presence of inter metallic compounds, hard zones and residual stresses may significantly degrade the dissimilar interface, making it prone to hydrogen induced cracking. Recently a series of failures on cathodically charged subsea dissimilar welds have been attributed to hydrogen embrittlement (HE), where the presence of carbide precipitates at the interface resulted in a microstructure particularly sensitive to hydrogen induced failures [9, 10]. Hydrogen induced degradation of mechanical properties is a well recognized threat in subsea structures and pipelines, with several reported incidents. It manifests as loss in toughness, which may result in unexpected and premature catastrophic failures. The basic mechanisms responsible for HE are still under debate, however two theories have advanced as the more accepted ones for the case of hydrogen degradation in steel: Hydrogen Enhanced Decohesion (HEDE), in which interstitial hydrogen reduces the bond strength and thus the necessary energy to fracture [11, 12]; and Hydrogen Enhanced Localized Plasticity (HELP), in which atomic hydrogen accelerates dislocation mobility through an elastic shielding effect which locally reduces the shear stress [13, 14]. Today it is seemingly

*Corresponding author
Email address: lise.jemblie@ntnu.no (L. Jemblie)
[1] Present address: Technip Norge AS, Grønøra Industriområde, 7300 Orkanger, Norway.

recognized that no single mechanism can comprehensively explain all the phenomena associated with HE, rather it appears that a combination of mechanisms is more likely in many cases.

The objective of the present study has been to investigate the fracture susceptibility and fracture behaviour of 316L austenitic stainless steel - X60/X65 carbon steel hot roll bonded clad pipes, both in air and with respect to hydrogen degradation. Bjaaland et al. [7] reported that the presence of a Ni-interlayer between the base material and the clad layer limits carbon diffusion across the interface, thereby preventing the formation of carbide precipitates and hard zones in the clad. The effect of an interface Ni-layer on the fracture susceptibility and degradation is therefore of special interest. Compact tension (CT) fracture mechanical testing has been performed in order to establish the crack growth resistance curves and fracture initiation toughness. For comparative reasons, values of the critical fracture toughness has also been determined. The fracture surfaces and fracture surface profiles has been investigated and related to the fracture toughness results.

2. Materials and Methods

2.1. Materials

Two different clad steel pipes are investigated in this study, presented in Table 1 as Sample A and Sample B respectively, with the main difference being the presence of a nickel interlayer between clad and base material for Sample A. The chemical composition and tensile properties are presented in Table 2.

Table 1: Investigated samples.

				Thickness [mm]	
	BM	Clad	Ni-interlayer	Clad	Pipe wall
Sample A	X65	316L	Yes	3.0	16.0
Sample B	X60	316L	No	3.0	15.7

The clad layer is bonded to the pipeline steel plate through hot rolling followed by quenching and tempering, before bent into the shape of a pipe in a press bending manufacturing process. Specimens for investigation were extracted in the longitudinal direction of the pipes in as supplied condition. The interface microstructure of both samples are presented in Figure 1. For Sample A, the 30-35 µm thick nickel interlayer is clearly visible, while nearly no carbide precipitates are visible. Sample B displays a continuous area of carbide precipitates (∼200 µm wide) on the clad side, attributed to carbon diffusion across the interface during production.

Microhardness profiles across the interface of both samples are presented in Figure 2, measured in the heat affect zone, 700 µm from the pipe girth weld. Sample B displays a hardness peak adjacent to the interface on the clad side and an abrupt drop in hardness adjacent to the interface on the BM side before a minimum value is attained, confirming carbon diffusion across the interface. For Sample A, no apparent hardness peak is visible on the clad side of the interface, while a minimum value on the BM side indicates some carbon diffusion towards the Ni-interlayer. The microhardness profile of Sample A is consistent with results by Missori et al. [4] and Dhib et al. [8] on hot roll bonded carbon steel-austenitic stainless steel clad plates. Bjaaland et al. [7] found that carbon diffusion mainly take place during the production process, with only minor contribution from the welding, confirming the validity of these results also for the un-welded case. A detailed interface characterization has previously been performed, and is reported in ref. [7, 15].

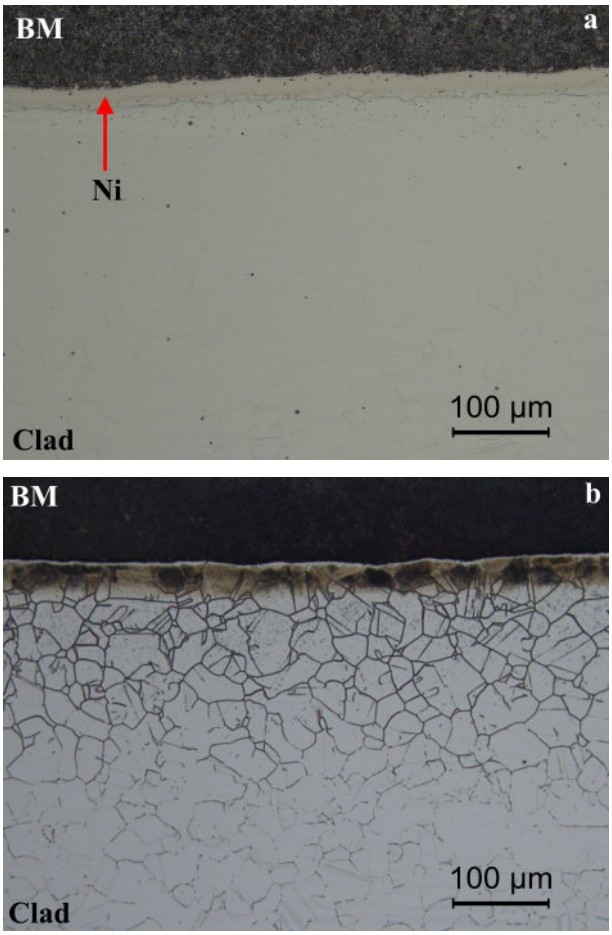

Figure 1: Interface microstructure of (a) Sample A and (b) Sample B [15].

2.2. Fracture mechanical testing

2.2.1. Experimental testing

Constant load rate CT fracture mechanical testing was performed in air and under cathodic protection (CP), in order to establish CTOD (Crack Tip Opening Displacement)-R curves and values for crack initiation. For comparative reasons, values of critical CTOD were also determined.

CT specimens were machined with the notch tip at the dissimilar metal interface to an initial crack length to width ratio a_0/W of 0.5, using electro-discharge machining

Table 2: Chemical composition and tensile properties of the clad steels under investigation.

	Steel	C	Si	Mn	P	S	Ni	Cr	Mo	Rp0.2 [MPa]	Rm [MPa]
Sample A	X65	0.07	0.13	1.48	0.007	0.0007	0.26	0.02	0.13	-	-
	316L	0.001	0.38	0.82	0.028	0.001	10.13	16.19	2.07	-	-
Sample B	X60	0.076	0.375	1.38	0.006	0.0008	0.27	0.024	0.003	493	595
	316L	0.018	0.368	1.382	0.031	0.002	11.09	16.68	2.042	440	647

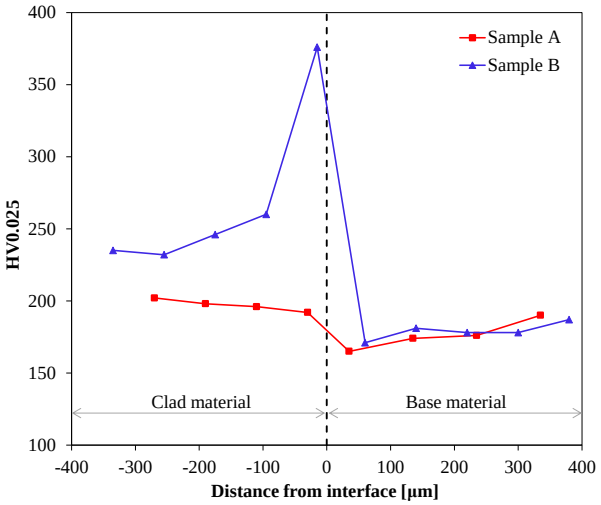

Figure 2: Vickers microhardness profiles across the interface of Sample A and Sample B.

(EDM), as it was deemed impossible to produce a fatigue crack propagating exactly along the dissimilar interface. Details of the specimen geometry and dimensions are given in Figure 3. Prior to machining, the samples were lightly etched in 2 % Nital to better reveal the dissimilar interface.

A constant loading rate of 0.74 N/min was applied, corresponding to a stress intensity rate of $6.8 \cdot 10^{-4}$ MPa $m^{1/2}/s$. This is in accordance with work by Lee and Gangloff [16] on hydrogen assisted cracking of ultra-high strength martensitic steel, making the resulting fracture toughness independent of the loading rate. For testing in hydrogen environment, the specimens were immersed in a 3.5 % NaCl solution with an applied cathodic potential of −1050 mV_{SCE}. Prior to test initiation, the specimens were hydrogen pre-charged in the test rig for 24 hours at −1050 mV_{SCE} in a 3.5 % NaCl solution. The charging conditions were maintained throughout the entire pre-charging and test period. Pre-charging time was decided by diffusion calculations in the BM, based on the thick plate solution of Fick's law. Using a diffusion coefficient equal to $2.50 \cdot 10^{-10}$ m^2/s experimentally measured on X70 pipeline steel, a hydrogen concentration level above 1.27 wppm was estimated throughout the BM, deeming 24 hours pre-charging time sufficient. All testing was performed at room temperature.

For determination of CTOD-R curves, a multiple specimen procedure was applied where the specimens were unloaded at different CTOD values in order to establish points on the curve for various crack extensions. The extent of stable crack growth was marked with heat tinting. After testing the samples were cracked open in liquid nitrogen, and the crack length and crack extension was measured at 5 equally spaced points across the sample, obtaining the original crack length a_0 and the mean crack extension Δa according to

$$a_0 = \frac{1}{4}\left(\frac{a_1 + a_5}{2} + \sum_{1=2}^{1=4} a_i\right) \quad (1)$$

$$\Delta a = \frac{1}{4}\left(\frac{\Delta a_1 + \Delta a_5}{2} + \sum_{1=2}^{1=4} \Delta a_i\right) \quad (2)$$

where a_1 and a_5 refers to the two measurements at the outer points. Due to non-uniform crack growth, the maximum crack extension for each sample was also measured.

2.2.2. Analysis of test data

During testing, the load and machine displacement were recorded. For testing in air, a machined clip gage, made to fit the small size of the specimen, was used to measure the Crack Mouth Opening Displacement (CMOD) at the knife edges. Due to the design of the fracture mechanical testing rig, it was not possible to use clip gages for testing under CP, where the specimen was immersed in a 3.5 % NaCl solution. Rather, the average ratio between plastic CMOD (V_p) and plastic displacement (d_p), resulting from testing in air, was used to obtain the plastic CMOD under CP

$$V_{p,\mathrm{CP}} = \left(\frac{V_{p,\mathrm{air}}}{d_{p,\mathrm{air}}}\right) \cdot d_{p,\mathrm{CP}} \quad (3)$$

at the point of maximum load for determination of critical CTOD and at the point of unloading for determination of the fracture resistance curves.

The CTOD values at maximum attained load were determined according to standard BS 7448-1 [17]. The CTOD-R curves were constructed following standard BS 7448-4 [18], with the fracture initiation toughness defined as the intersection between the R-curve and the analytical blunting line ($\delta = 1.87(R_m/R_{p0.2})\Delta a$).

Fracture surfaces and fracture profiles were examined using a combination of light optical microscopy (LOM) and scanning electron microscopy (SEM).

3. Results

3.1. Fracture resistance curve and values for crack initiation

The typical CT fracture surfaces after heat tinting are displayed in Figure 4, illustrating the evolvement of the

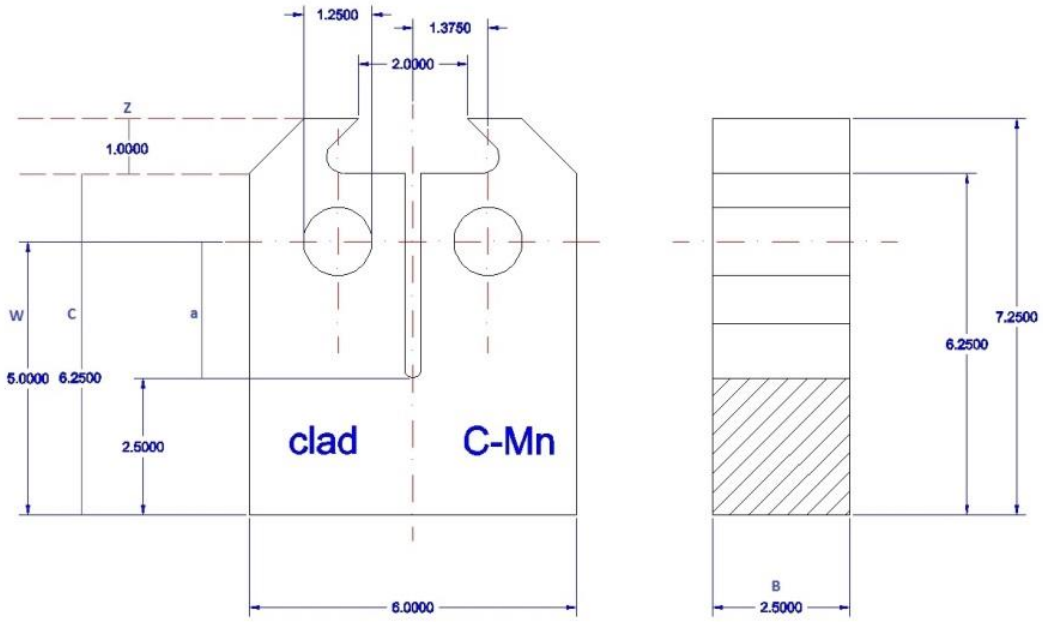

Figure 3: Compact tension specimen geometry and dimensions, W=5 mm, B=2.5 mm, a=2.5 mm, C=6.25 mm, z=1.0 mm, notch radius=0.15 mm.

crack with increasing CTOD level. Non-uniform crack extension and crack tunneling was observed for all samples, irrespective of environment.

The resulting linear best fit crack growth resistant curves are compared in Figure 5 and 6, illustrating a significant influence of hydrogen on Sample B, with little to no hydrogen influence on Sample A. Due to the extent of non-uniform crack extension, the CTOD values were calculated both in terms of the mean crack extension according to Equation 2 and in terms of the measured maximum crack extension ($\Delta a_{\max}$).

The fracture initiation toughness, determined from the crack growth resistant curves, are summarized in Table 3 and 4. As the J-integral and the stress intensity factor are more commonly cited fracture mechanical parameters, the values of the CTOD fracture initiation toughness were converted to J and K_I. Hydrogen was found to reduce the CTOD fracture initiation toughness with 20 % for Sample A and 85 % for Sample B in the case of mean crack extension, and with 50 % and 94 %, respectively, in the case of maximum crack extension.

Table 3: Fracture initiation toughness in terms of mean crack extension.

	Env.	δ_i [mm]	$J^{a)}$ [N/mm]	$K_I^{b)}$ [MPa$\sqrt{m}$]
A	Air	0.099	97	149
A	CP	0.079	78	133
B	Air	0.176	173	199
B	CP	0.025	25	76

a) $J = 2\delta R_{p0.2}$

b) $K_I = \left(\frac{JE}{1-\nu^2}\right)^{1/2}$

Table 4: Fracture initiation toughness in terms of maximum crack extension.

	Env.	δ_i [mm]	$J^{a)}$ [N/mm]	$K_I^{b)}$ [MPa$\sqrt{m}$]
A	Air	0.080	79	134
A	CP	0.040	39	95
B	Air	0.142	140	179
B	CP	0.008	8	42

a) $J = 2\delta R_{p0.2}$

b) $K_I = \left(\frac{JE}{1-\nu^2}\right)^{1/2}$

3.2. Critical CTOD

The results in terms of CTOD (δ) at maximum attained load are reported in Table 5 and 6 for Sample A and Sample B, respectively, and graphically in Figure 7. When comparing Sample A and Sample B, it was observed that Sample B displayed a higher CTOD and plastic CMOD level for testing in air than Sample A, with no variation in terms of maximum attained load, indicating more plastic deformation prior to failure.

For Sample A, fairly consistent values of both maximum load and corresponding CTOD was observed, irrespective of environment, with a mean reduction in CTOD of 8% indicating again little to no hydrogen influence. Sample B displayed again significant influence of hydrogen on the fracture toughness, with a mean reduction in CTOD of 77%.

3.3. Fractorgraphy

In order to verify the influence of hydrogen on the fracture, selected samples were investigated in SEM, see Figure 8. The results appeared consistent for all parallel tests.

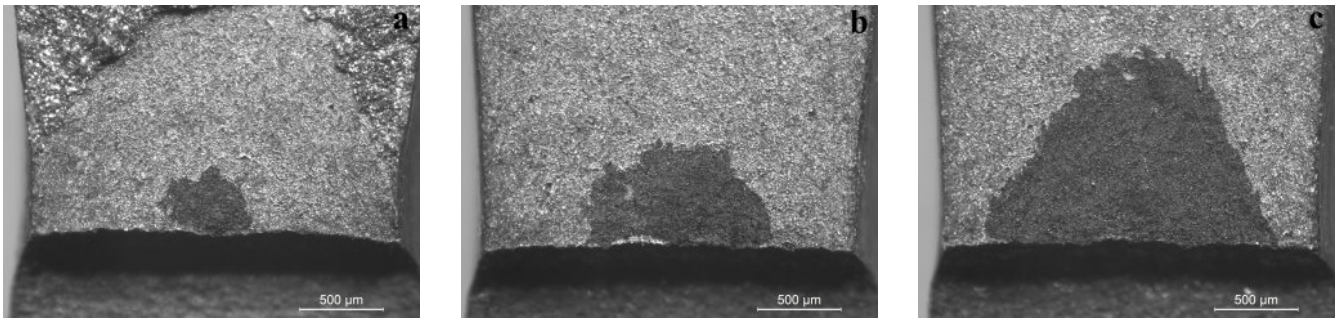

Figure 4: Typical CT fracture surfaces after heat tinting, illustrating the evolvement of the crack with increasing CTOD level. The dark regions represent the crack extension areas. (a) Sample A02. (b) Sample A05. (c) Sample A03.

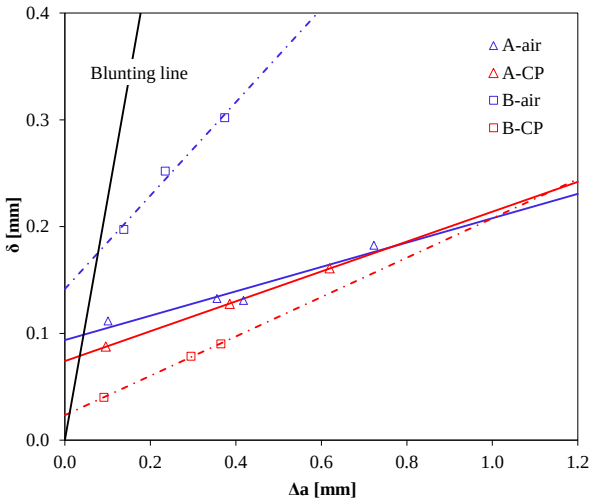

Figure 5: Linear best fit CTOD-R curves, calculated in terms of mean crack extension. Sample A and B for tests in air and under CP.

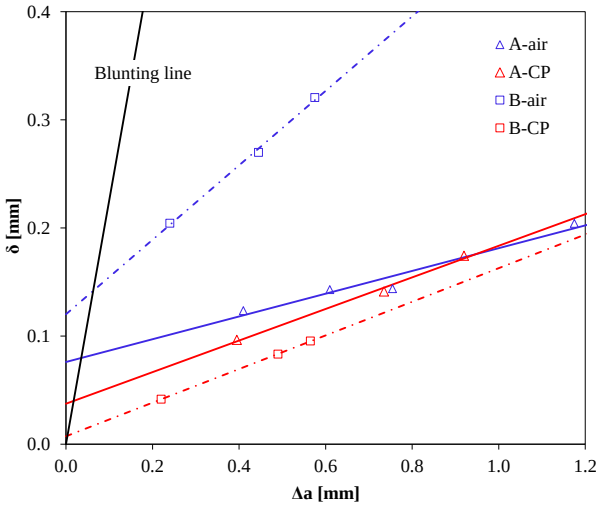

Figure 6: Linear best fit CTOD-R curves, calculated in terms of maximum crack extension. Sample A and B for tests in air and under CP.

The fracture surfaces of the samples tested in air (both Sample A and B) revealed a dimpled morphology, indica-

Table 5: Results at maximum attained load for fracture mechanical testing of Sample A.

Sample	Environment	F_{max} [N]	V_p [mm]	δ_m [mm]
A01	Air	729	0.566	0.115
A02	Air	693	0.530	0.105
A03	Air	710	0.538	0.108
A04	Air	710	0.484	0.098
A05	Air	718	0.542	0.108
A06	CP	752	0.592	0.121
A07	CP	721	0.486	0.097
A08	CP	686	0.401	0.082
A09	CP	687	0.470	0.094
A10	CP	676	0.479	0.096

Table 6: Results at maximum attained load for fracture mechanical testing of Sample B.

Sample	Environment	F_{max} [N]	V_p [mm]	δ_m [mm]
B01[a)]	Air	724	0.961	0.192
B02	Air	718	0.981	0.194
B03	Air	684	0.904	0.179
B04	Air	705	1.017	0.199
B05	Air	714	1.041	0.201
B06	CP	634	0.245	0.053
B07	CP	620	0.167	0.037
B08	CP	630	0.152	0.035
B09	CP	662	0.227	0.049
B10	CP	639	0.213	0.046

a) Loading rate: 10 N/min

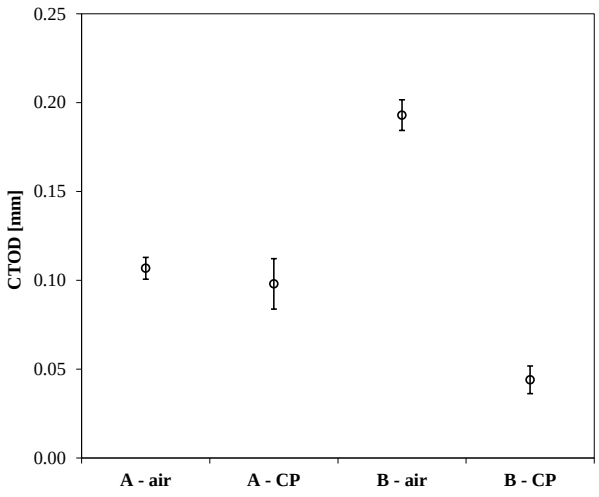

Figure 7: Values of critical CTOD at maximum attained load for fracture mechanical testing of Sample A and Sample B.

tive of ductile fracture. For Sample B tested under CP, the fracture surface revealed a clear influence of hydrogen; a distinct multifaceted appearance, indicative of cleavage fracture, followed by a quasi-cleavage fracture morphology. This corresponds to the strong loss in ductility observed for this sample when tested under CP, quantified by the lowered CTOD values reported in Table 6 and 3. For Sample A tested under CP, the fracture surface revealed two fracture morphologies existing on two distinct elevations (Figure 8e). The initial lower part of the fracture surface had a quasi-cleavage appearance, while the elevated part, approximately 100 µm into the length of the crack, had a dimpled morphology, indicative of ductile fracture.

In order to determine the fracture path, the fracture surface profiles of selected samples were examined in LOM. The results, which appeared consistent for all parallel tests, are presented in Figure 9. For Sample A, the fracture profiles revealed that the crack propagated along the BM-Ni interface, slightly into the Ni-interlayer, for testing in air. For testing under CP, the crack initiated approximately 50 µm into the BM, indicating hydrogen influence, followed by propagation along the BM-Ni interface, slightly into the Ni-interlayer, see Figure 9a and 9b. This is consistent with the observation of two distinct elevations on the fracture surface for this sample. The Ni-interlayer is visible as the pale, featureless band located above the BM microstructure. For Sample B, the fracture profiles revealed an alternating crack path, shifting between the dissimilar interface and the BM adjacent to the interface, for both test environments, with the crack propagating slightly more into the BM for the samples tested in air.

4. Discussion

4.1. Fracture toughness

The results from testing in air reveal a significant influence of material combination on the fracture resistance, with a mean reduction in CTOD of 44 % for Sample A compared to Sample B. Commercially pure nickel yields at about 180 MPa ($R_{p0.2}$), well below the yield limit for steel, also considering softening due to decarburization in the BM adjacent to the interface. Thus, the Ni-interlayer represents a soft zone, preferable for crack propagation, consequently lowering the fracture toughness. For Sample B, fracture in the decarburization region of the BM is consistent with findings from Shushan et al. [3] and Vigraman et al. [6] on diffusion bonded stainless steel to carbon steel, attributed to grain growth and softening during the bonding process.

The results from testing under CP reveal overall low influence of hydrogen on the fracture toughness of Sample A. This is caused by crack propagation mainly in the Ni-interlayer, which displays no influence of hydrogen on the fracture surfaces. A observation consistent with the low diffusivity and high solubility of hydrogen in nickel. Hillier and Robertson [19] found that an electroplated Ni-interlayer in itself acts as a barrier to hydrogen diffusion, thus limiting embrittlement in the underlying steel. The influence of hydrogen is however apparent when evaluating the initial crack path, indicating a distinct effect of hydrogen on the BM. This is consistent with the observed lowering of the fracture initiation toughness values, where a shift in crack initiation site would consequently lower the fracture toughness compared to the unembrittled case. Hydrogen degradation of the ferritic BM is consistent with the general knowledge of hydrogen effects on pipeline steels. Comparing the CTOD-R curves of Sample A, it is apparent that the samples tested under CP demonstrates a steeper curve. This is surprising as hydrogen is known to lower the resistance to additional crack growth and consequently reduce the CTOD-R curve slope [20], indicating a discrepancy in the results for realistically quantifying the effect of hydrogen on Sample A. Based on the fracture profiles, both curves are expected to yield similar steepening, while crack growth mainly occurs in the Ni-interlayer.

Sample B is found strongly susceptible to hydrogen embrittlement, with the degradation of the ferritic BM consistent with general knowledge of hydrogen effects on pipeline steels. The alternating crack path could indicate lack of bonding resulting from the production. Micrographs of the samples do illustrate the presence of discontinuities along the interface of Sample B, which are not visible in Sample A [15]. Another possibility is the presence of two "competing" low energy fracture zones; the coarse grained BM and the interface, degraded by the presence of carbide precipitates and residual stresses. It is well known that hydrogen is prone to accumulate at precipitates and to enhance the formation of voids [9]. The presence of carbides was found to be the main cause of a series of hydrogen related failures on cathodically charged subsea AISI 8630-IN625 dissimilar welds, making the weld more susceptible to hydrogen embrittlement by providing a low energy fracture path [9, 10]. It was further emphasised that the density and distribution of carbides, and thus the susceptibility to hydrogen embrittlement, was strongly dependent on the production conditions. Milititsky et al. [21] have performed SENB (single edge notched bend) fracture toughness testing on AISI 8630-IN625 dissimilar metals welds and found that hydrogen reduced the mean $J_{0.2}$ fracture initiation toughness with 86 %, consistent with the results for Sample B. The present study, however, demonstrates a steeper R-curve, indicating larger resistance to additional crack growth. It should be noted that the time frame for the pre-charging period was decided based on diffusion calculations in the BM, attaining a nearly uniform hydrogen concentration level throughout the base material. Conforming to the thick plate solution of Fick's law, using a hydrogen diffusion coefficient equal to $2.2 \cdot 10^{-16}$ m^2/s representative of austenitic stainless steel, a hydrogen diffusion distance less than 30 µm from the surface is estimated in the clad. With increased pre-charging time, the propensity for hydrogen to accumulate at precipitates could possibly infer hydrogen embrittlement in the clad.

Comparing Sample A and B for testing under CP, the

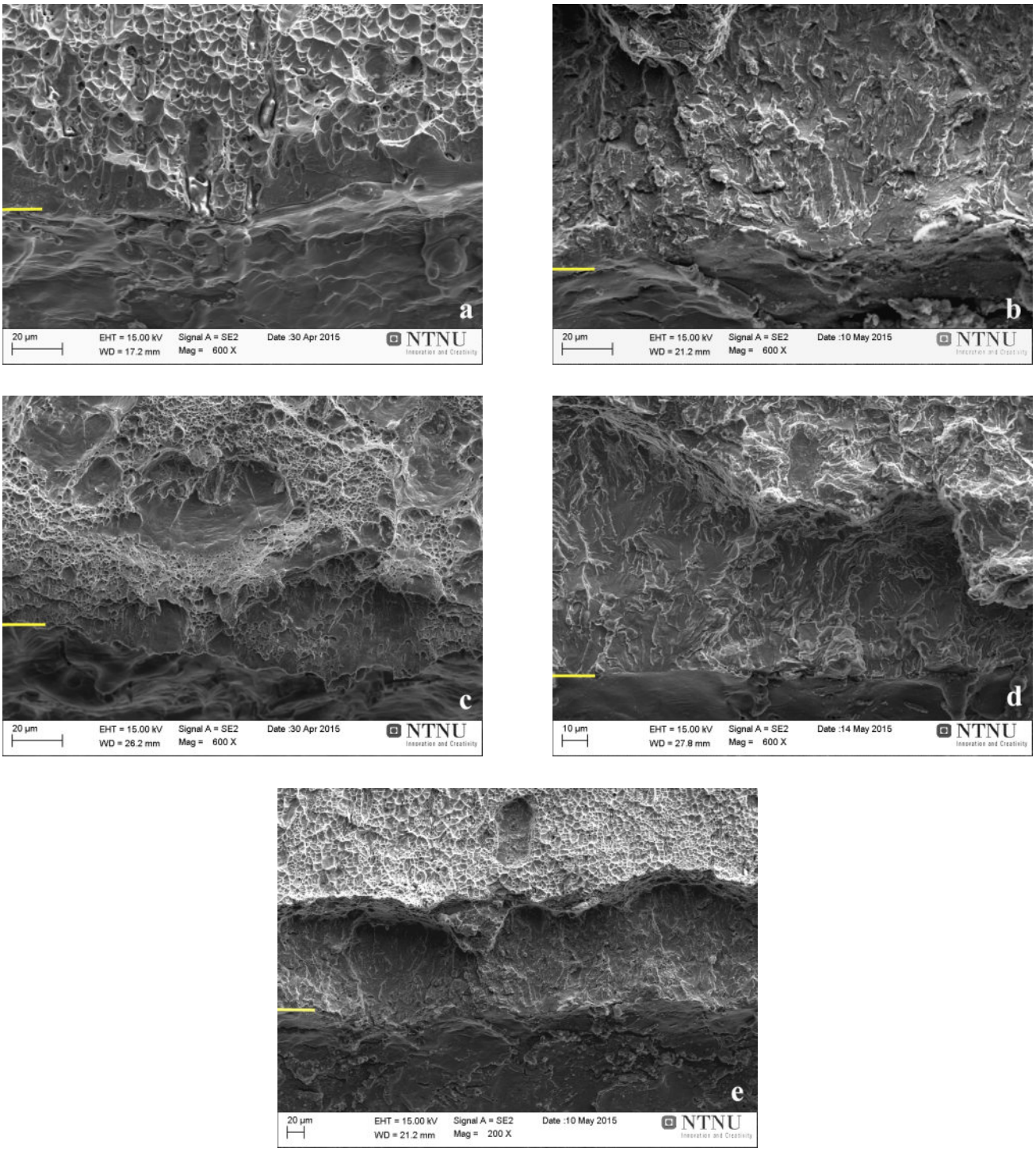

Figure 8: Fracture surfaces of the CT samples. The yellow line indicate the end of the EDM notched area, with the fracture surface above the line. All images are taken from the BM side of the cracked specimen. (a) Sample A tested in air. (b) Sample A tested under CP. (c) Sample B tested in air. (d) Sample B tested under CP. (e) Sample A tested under CP, reduced magnification.

presence of a Ni-interlayer raises the fracture initiation toughness with 216 %. It is noteworthy that the fracture resistance of Sample B falls below that of Sample A, indicating more resistance towards hydrogen cracking in the BM of Sample A compared to that of Sample B. If the resistance was the same, also Sample A tested under CP would fracture in the BM. This illustrates the effect of material combination on the fracture toughness, where the carbon depleted, coarse grained BM of sample B appear more prone to hydrogen embrittlement. While electroplated nickel limits element diffusion and thus increases the resistance to hydrogen degradation and cracking, the

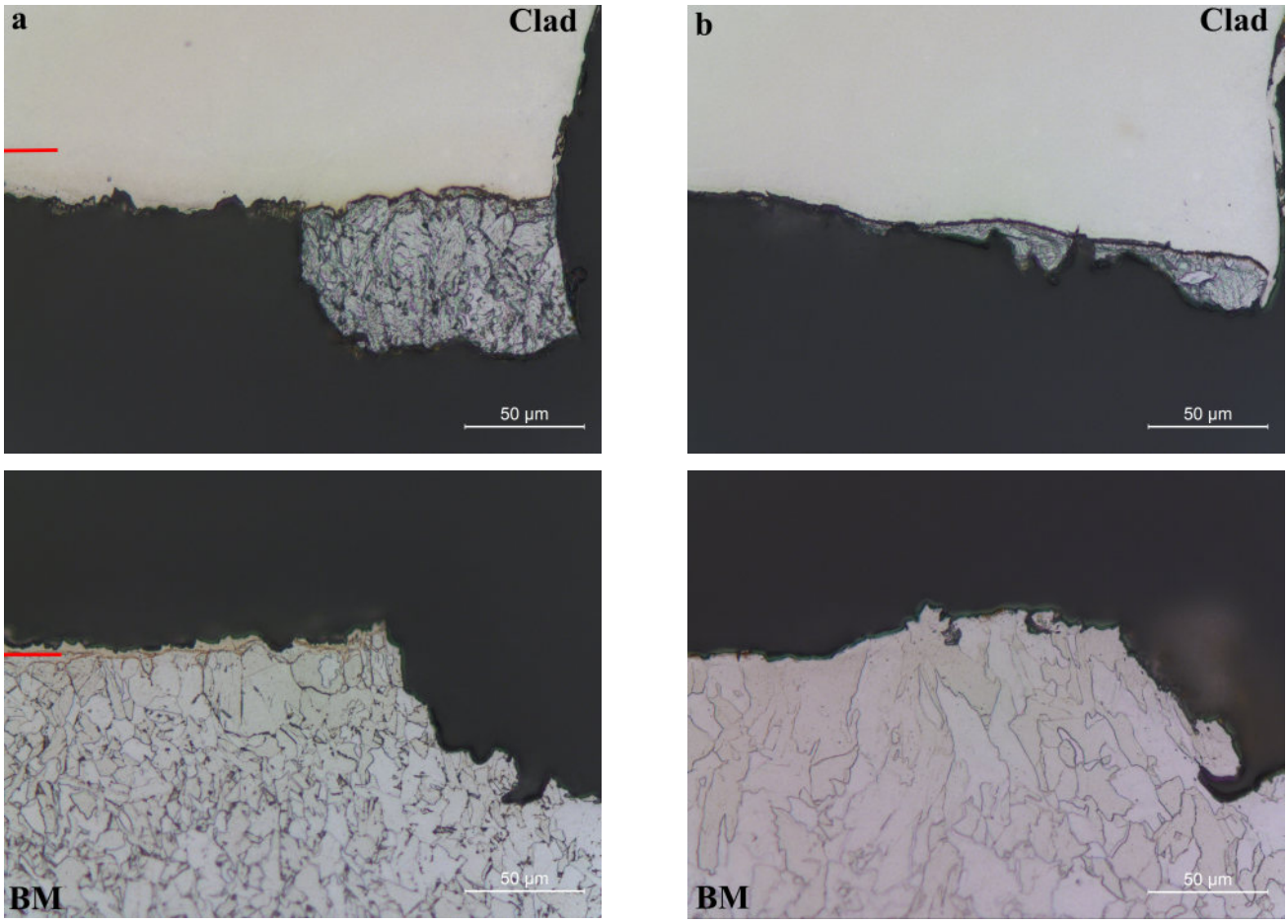

Figure 9: LOM micrographs showing the fracture profile of the CT samples tested under CP. (a) Sample A, the upper image displays the clad part of the fracture path and the lower image displays the BM part. The Ni-interlayer is indicated by a red line in both images. (b) Sample B, the upper image displays the clad part of the fracture path and the lower image displays the BM part.

Ni-interlayer itself represents a zone preferable for crack propagation, consequently lowering the overall fracture resistance of the system.

4.2. Effect of specimen size and geometry

Due to the thickness of the clad layer being only 3 mm, the sample specimens were dimensioned accordingly, inferring fracture toughness values outside the standardized valid range. Thus, the resulting fracture toughness values obtained in the present work should mainly be viewed as a relative comparisons between materials and environments, not absolute values. Additionally, the samples were notched by EDM rather than fatigue pre-cracking, as it was deemed not feasible to introduce a fatigue crack propagating exactly along the interface. In the fracture toughness tests on AISI 8630-IN625 dissimilar metals welds performed by Milititsky et al. [21], samples with fatigue precracks displayed lower fracture toughness values compared to samples notched by EDM. It is expected that a blunted notch will result in less conservative fracture toughness results compared to a sharp crack, especially for low fracture toughness values.

A large extent of non-uniform crack extension and crack tunneling was observed for all samples, independent of material and environment, indicating a probable geometrical cause. From a fracture mechanical point of view, crack tunneling will occur if the operating fracture criterion is first met in the mid section of the crack front, which may be due to a higher fracture driving force or a lower fracture toughness in this area [22, 23]. The extent of crack tunneling may generally infer less conservative fracture resistance curves when calculated in terms of mean crack extension, with little to no crack growth at the outer points of Equation (2). Comparing with the results in terms of maximum crack extension, a lowering of the fracture initiation toughness of 19 % was observed for the samples tested in air and 49 - 69 % for sample A and B tested under CP, in addition to a general reduction in the R-curve slope.

5. Conclusion

Constant load rate fracture mechanical testing has been preformed in air and under CP in order to evaluate the effect of material and environment on the fracture susceptibility and fracture behaviour of 316L - X60/X65 carbon

steel hot roll bonded clad pipes. The main results are summarized as follows:

- The highest fracture toughness was obtained for the samples without a Ni-interlayer tested in air, followed by the samples with a Ni-interlayer tested in air and under CP. The lowest fracture toughness was obtained for the samples without a Ni-interlayer tested under CP.
- The presence of a Ni-interlayer reduced the fracture initiation toughness with 44 % for testing in air, while it raised the fracture initiation toughness with 216 % for testing under CP.
- The samples with a Ni-interlayer revealed low susceptibility to hydrogen embrittlement, with a reduction in the fracture initiation toughness of 20 %.
- The samples without a Ni-interlayer revealed a clear influence of hydrogen on the fracture resistance, with a reduction in the fracture initiation toughness of 85 %.
- Fracture occurred mainly in the nickel for the samples with a Ni-interlayer. In the presence of hydrogen, fracture initiated in the base metal followed by propagation in the Ni-interlayer.
- The samples without a Ni-interlayer revealed an alternating crack path, shifting between the dissimilar interface and the base metal adjacent to the interface for both environments.

Acknowledgements

The present work was financed by the Research Council of Norway (Petromaks 2 programme, Contract No. 234110 /E30), Statoil, Gassco, Technip, POSCO and EDF Induction and performed within the frames of the ROP project (www.sintef.no/rop).

References

[1] L. Smith, M. Celant, CASTI handbook of cladding technology, 2nd Edition, CASTI Publishing Inc., 2000.

[2] T. Reichel, J. Beissel, V. Pavlyk, G. Heigl, Production of metallurgically cladded pipes for high end applications in the oil & gas industry, in: Proc. ASME 27th Int. Conf. Offshore Mech. Arct. Eng., 2008, pp. 179–186.

[3] S. M. Shushan, E. A. Charles, J. Congleton, The environment assisted cracking of diffusion bonded stainless to carbon steel joints in an aqueous chloride solution, Corros. Sci. 38 (5) (1996) 673–686. doi:10.1016/0010-938X(96)00158-8.

[4] S. Missori, F. Murdolo, A. Sili, Microstructural characterization of a stainless-cladded carbon steel, Metall. Sci. Technol. 19 (2) (2001) 21–24.

[5] B. Kurt, A. Çalik, Interface structure of diffusion bonded duplex stainless steel and medium carbon steel couple, Mater. Charact. 60 (9) (2009) 1035–1040. doi:10.1016/j.matchar.2009.04.011.

[6] T. Vigraman, D. Ravindran, R. Narayanasamy, Diffusion bonding of AISI 304L steel to low-carbon steel with AISI 304L steel interlayer, Mater. Des. 34 (2012) 594–602. doi:10.1016/j.matdes.2011.05.012.

[7] H. Bjaaland, O. M. Akselsen, V. Olden, B. Nyhus, M. Karlsen, J. Hjelen, Metallurgical reactions in welding of clad X60 / X65 pipelines, Proc. Twenty-fifth Int. Ocean Polar Eng. Conf. (2015) 61–66.

[8] Z. Dhib, N. Guermazi, M. Gaspérini, N. Haddar, Cladding of low-carbon steel to austenitic stainless steel by hot-roll bonding: Microstructure and mechanical properties before and after welding, Mater. Sci. Eng. A 656 (2016) 130–141. doi:10.1016/j.msea.2015.12.088.

[9] J. A. Fenske, I. M. Robertson, R. Ayer, M. Hukle, D. Lillig, B. Newbury, Microstructure and hydrogen-induced failure mechanisms in Fe and Ni alloy weldments, Metall. Mater. Trans. A 43 (9) (2012) 3011–3022. doi:10.1007/s11661-012-1129-1.

[10] M. F. Dodge, H. B. Dong, M. F. Gittos, T. Mobberley, Fusion zone microstructure associated with embrittlement of subsea dissimilar joints, Proc. ASME 33rd Int. Conf. Ocean. Offshore Arct. Eng. 5. doi:10.1115/OMAE2014-23643.

[11] A. R. Troiano, The role of hydrogen and other interstitials in the mechanical behaviour of metals, Trans. ASM 52 (1960) 54–80.

[12] R. A. Oriani, A mechanistic theory of hydrogen embrittlement of steels, Berichte der Bunsengesellschaft für Phys. Chemie 76 (8) (1972) 848–857. doi:10.1002/bbpc.19720760864.

[13] H. Birnbaum, P. Sofronis, Hydrogen-enhanced localized plasticitya mechanism for hydrogen-related fracture, Mater. Sci. Eng. A 176 (1-2) (1994) 191–202. doi:10.1016/0921-5093(94)90975-X.

[14] I. M. Robertson, H. K. Birnbaum, P. Sofronis, Chapter 91 Hydrogen effects on plasticity, Dislocations in Solids 15 (2009) 249–293. doi:10.1016/S1572-4859(09)01504-6.

[15] A. S. Azar, Characterization of Oil & Gas Clad Pipelines, Tech. Rep. SINTEF A26507, SINTEF Materials and Chemistry (2014).

[16] Y. Lee, R. P. Gangloff, Measurement and modeling of hydrogen environment–assisted cracking of ultra-high-strength steel, Metall. Mater. Trans. A 38 (13) (2007) 2174–2190. doi:10.1007/s11661-006-9051-z.

[17] British Standard BS 7448-1, Fracture mechanics toughness tests - Part 1: Method for determination of KIc, critical CTOD and critical J values of metallic materials (1991).

[18] British Standard BS 7448-4, Fracture mechanics toughness tests - Part 4: Method for determination of fracture resistance curves and initiation values for stable crack extension in metallic materials (1997).

[19] E. Hillier, M. Robinson, Hydrogen embrittlement of high strength steel electroplated with zinccobalt alloys, Corros. Sci. 46 (3) (2004) 715–727. doi:10.1016/S0010-938X(03)00180-X.

[20] B. P. Somerday, M. Dadfarnia, D. K. Balch, K. A. Nibur, C. H. Cadden, P. Sofronis, Hydrogen-Assisted crack propagation in austenitic stainless steel fusion welds, Metall. Mater. Trans. A Phys. Metall. Mater. Sci. 40 (10) (2009) 2350–2362. doi:10.1007/s11661-009-9922-1.

[21] M. Mililitsky, M. F. Gittos, S. E. Smith, V. Marques, T. Ltd., Assessment of Dissimilar Metal Interfaces for Sub-Sea Application under Cathodic Protection, in: Proc. from Mater. Sci. Technol. Conf., MS&T Partner Societies, 2010, pp. 2484–2495.

[22] J. Zuo, M. A. Sutton, X. Deng, C. S. Cheng, Crack tunneling: effect of stress constraint, in: Proc. IMECE04 2004 ASME Int. Mech. Eng. Congr. Expo., 2004, pp. 393–400.

[23] W. Lan, X. Deng, M. A. Sutton, Investigation of crack tunneling in ductile materials, Eng. Fract. Mech. 77 (14) (2010) 2800–2812. doi:10.1016/j.engfracmech.2010.06.010.